Bull. Mater. Sci. (2018) 41:107
https://doi.org/10.1007/s12034-018-1620-4

Morphology-controlled ultrafine $BaTiO_3$-based PVDF–HFP nanocomposite: synergistic effect on dielectric and electro-mechanical properties

VAIBHAV KHIRATKAR, RADHAMANOHAR AEPURU and H S PANDA*
Department of Materials Engineering, Defence Institute of Advanced Technology, Pune 411025, India
*Author for correspondence (himanshusp@diat.ac.in; hspanda3@gmail.com)

MS received 31 May 2017; accepted 6 December 2017; published online 27 July 2018

Abstract. Perovskite-based flexible nanocomposites were realized by dispersing $BaTiO_3$ and modified monodisperse $BaTiO_3$ in PVDF–HFP matrix. $BaTiO_3$ was modified *in situ* by the addition of carbon solution, which was prepared electrochemically by using graphite rod. Structural characterization revealed that the decrease in tetragonality due to reduction in particle size of modified $BaTiO_3$ than unmodified $BaTiO_3$. The controlled morphology of treated-$BaTiO_3$ nanoparticles was well dispersed in polymer matrix and exhibited effective dielectric constant. High active surface area of modified $BaTiO_3$ suggested strong interfacial polarization, reduced dielectric loss and induced relaxation as compared to PVDF–HFP/BT nanocomposite. The experimental dielectric behaviour was fitted with theoretical Maxwell–Garnet model and composites followed up to 20 wt.% filler. The polarization effect was further proven by electric modulus studies of nanocomposites in broad frequency (0.1 Hz–1 MHz) and temperature (-40 to 130°C). The results suggested that the shift in relaxation peaks towards higher frequencies with increase in filler content in polymer matrix. Further, a flexible-pressure sensing device was fabricated and evaluated for real applications.

Keywords. Polygonal; barium titanate; hydrothermal; dielectric; sensor.

1. Introduction

Ferroelectric ceramics with high permittivity are potential candidates for numerous applications, such as energy storage and conversion devices. In general, the ferroelectricity of ceramics depends on the symmetry of the crystal structure and their dielectric properties. In this aspect, the dielectric studies were carried out in various ceramics, such as lead-based titanate and lead-free ceramics [1,2]. Among the lead-free ceramics, $BaTiO_3$ has highest ferroelectric properties in its non-centrosymmetric structure and can be tuned further by substituting various dopants (Sr, Ca and Zr) [3,4]. Numerous processes such as hydrothermal, solid-state, co-precipitation and sol–gel are employed to synthesize $BaTiO_3$ to modify the morphology and size [2,3]. Amongst, hydrothermal method provides better control over size, morphology and crystalinity with low temperature requirement than other methods [5]. Conventional hydrothermally formed $BaTiO_3$ changes from spherical nuclei formation to cubical intermediate shape due to growth in habit plane, and finally, stabilizes in spherical shape due to the dissolution of high energy cubic edges [6]. These perovskite ceramics possess high dielectric constant due to permanent dipole moment and alignment of this dipole in the direction of applied electric field [4]. These ceramics have higher dielectric constant, but low breakdown strength and highly brittle in nature [7]. To overwhelm, ferroelectric ceramic–polymer nanocomposites are realized to improve the dielectric properties by combining high permittivity ceramics with mechanically flexible, high breakdown strength and easy processing polymers [8]. Ferroelectric polymers, such as poly(vinylidene fluoride) (PVDF) and its co-polymers, such as trifluoroethylene (TrFE) and hexafluoroethylene (HFP) exhibit higher dielectric properties due to the presence of electronegative fluorine, which gives rise to crystalline phases [9].

On the other hand, dielectric performance of nanocomposite depends on the percentage of ceramic fillers, dispersion and their microstructures. However, large percentage of ceramic inclusion in the polymer matrix enhanced dielectric constant with decreased breakdown strength and mechanical properties [10–12]. Recently, few strategies were employed to enhance the dielectric constant at low filler content with various forms of fillers [13–18]. One of them is surface modification of the ceramic particle with surfactant to get better dispersion in polymer matrix. In this context, work was carried out by surface modification of $BaTiO_3$ nanoparticles using water-soluble polyvinylpyrrolidone (PVP) in PVDF matrix [19]. On the other hand, to enhance the dielectric properties, addition of conducting fillers, such as carbon-based nanofillers (activated carbon, CNTs, graphene, etc.) were reported to prepare percolative nanocomposites with low filler content associating to percolation theory [20,21].

The major concern in these composites is high dielectric loss arising from high leakage currents [20]. In addition, aggregation of fillers in the polymer matrix also tends to increase dielectric loss due to the formation of voids in the polymer ceramics composite. This aggregation of ceramic particles in polymer matrix can be reduced by the preparation technique of composite [22]. Therefore, we hypothesize to modify $BaTiO_3$ to get better dispersion in polymer matrix, which can enhance the permittivity with low dielectric loss improving the dielectric and electro-mechanical properties.

In this study, we have shown evolution of polyhedral morphology of $BaTiO_3$ by adopting surfactant-assisted hydrothermal synthesis. The developed nanofillers were incorporated in PVDF–HFP matrix to make nanocomposite films and the structural and dielectric properties were studied. Morphological study suggested the formation of polygonal-shaped $BaTiO_3$. Dielectric studies of nanocomposite films revealed the improvement in the dielectric properties of fillers with varying concentrations. Again, we miniaturize $BaTiO_3$ fillers by adding carbon during the synthesis to modify the surface, which significantly enhanced the permittivity and simultaneously reduce the dielectric loss of PVDF–HFP nanocomposite. Further, experimental dielectric values are correlated with theoretical Maxwell–Garner model. Also, capacitive pressure sensor response was investigated, which suggested the improvement in sensing the response of nanocomposite than pure polymer under applied loads.

2. Experimental

2.1 *Synthesis of $BaTiO_3$ nanoparticles*

In a typical process, one gram polyethelylene glycol (PEG) 400 (Loba chemie) was mixed in 10 ml ethanol under stirring for 15 min. One millimole of titanium (IV) n-butoxide (TBOT) (Alfa Aesar, ≥98%) in 10 ml ethanol was added to PEG mixture and continued stirring for 15 min. Thereafter, 2 M KOH solution (10 ml) and 1 mmol $Ba(OH)_2{\cdot}8H_2O$ (Kemphasol, 98%, 0.315 g in 10 ml deionized water) were added to the above mixture. The complete mixture was vigorously stirred for 30 min and transferred to a Teflon-lined stainless steel autoclave. The autoclave was heated to 200°C for 16 h and then cooled to room temperature. The obtained solution was washed with formic acid (0.1 M), ethanol and deionized water several times to remove impurities. Separated precipitates are dried at 60°C for overnight and used for characterization.

2.2 *Synthesis of modified $BaTiO_3$ nanoparticles*

Modified $BaTiO_3$ was prepared *in situ* by adding carbon solution, which was previously synthesized by using electrochemical method [23]. In summary, the electrolyte was prepared by mixing ethanol/H_2O (volume ratio = 99 : 1) with 0.3 g NaOH. Graphite rods (dia. 8 mm) were used as electrodes. The electrochemical process was continued for 1 h with current intensity ranging from 100 to 200 mA cm^{-2} to obtain carbon solution. Five millilitres of the above prepared carbon solution was added to base solution to modify $BaTiO_3$ according to the above mentioned process.

2.3 *Preparation of nanocomposite films*

Nanocomposite films were prepared by using solvent-casting method. Initially, poly(vinylidene fluoride-co-hexafluoropropylene) (Sigma, Aldrich) was dissolved in dimethylformamide (DMF) under stirring. Then, various wt.% of $BaTiO_3$ and modified $BaTiO_3$ were added to the polymer solution separately and sonicated to get homogeneous dispersion. The mixture was poured in a Petri dish and dried at 65°C for overnight to obtain the composite film.

2.4 *Characterization*

The crystal structure of $BaTiO_3$ (BT) and modified $BaTiO_3$ (CBT) were identified by powder X-ray diffraction (XRD) (BRUKER D8 Advance) with CuKα radiation ($\lambda = 1.542$ Å) and with a scanning range of (2θ) 10–80°. Structural analysis was carried out spectroscopically by using Raman spectroscopy (Lab RAM HR (800), HORIBA Scientific with Olympus BX41) with solid-state laser excitation wavelength of 632 nm to confirm the modification process. The morphology of $BaTiO_3$ and nanocomposite film were identified by field emission scanning electron microscope (Sigma, Carl Zesis). Dielectric properties of $BaTiO_3$ and nanocomposites were measured by using Novocontrol broad band dielectric spectrometer with attached Alpha-A high frequency analyzer and temperature controller. The samples were coated with quick drying silver paste on both sides and they were placed between gold-plated electrodes to measure dielectric properties.

3. Results and discussion

3.1 *Structural studies*

XRD patterns are indexed and matched with JCPDS no. 05-626 with lattice constant $a = 3.89$ Å, $c = 4.038$ Å and space group of P_{4mm} (figure 1a), which confirmed the formation of single phase $BaTiO_3$. Triplet splitting of (002) plane represented the simultaneous extension and compression along the c-axis, and suggested the presence of tetragonal and orthorhombic phases in $BaTiO_3$ (figure 1b). The corresponding pseudo-cubic (002) plane was also observed at $2\theta \sim 45°$ and shown in figure 1b. Fraction of tetragonal (F_T) and orthorhombic (F_O) phases was calculated by using the intensity of overlapping peaks $F_{T(200)}$, $F_{T(002)}$ and $F_{O(200)}$ between angles $45° \leq 2\theta \leq 47°$ by using least square refinement with Lorentzian profile function to know the asymmetricity of $BaTiO_3$ [24]. The fraction of tetragonal and orthorhombic

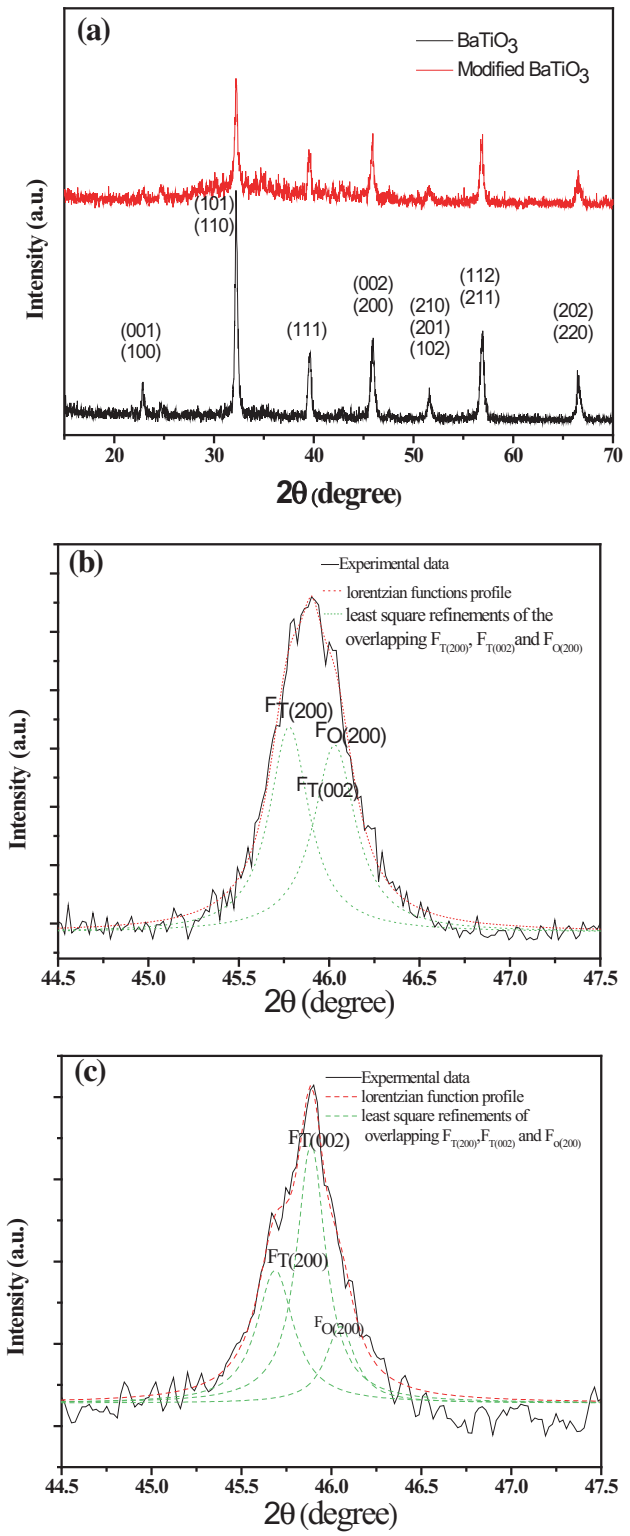

Figure 1. XRD patterns of (**a**) $BaTiO_3$ and modified $BaTiO_3$, (**b**) Lorentzian profile fitting of XRD in $BaTiO_3$ and (**c**) Lorentzian profile fitting of XRD in modified $BaTiO_3$.

phases was calculated to be around 65 and 35% for $BaTiO_3$ and 84 and 16% for modified $BaTiO_3$, respectively. Decrease

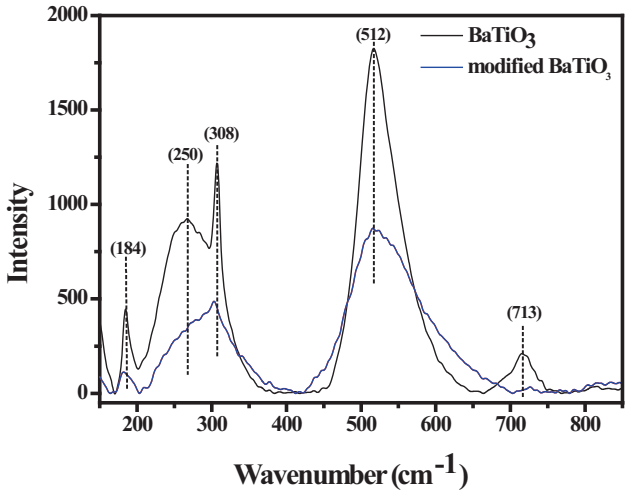

Figure 2. Raman spectra of $BaTiO_3$ and modified $BaTiO_3$.

in intensity of XRD patterns suggested the reduction in particle size, which further confirmed by the microscopic studies. Also, the shift in peaks represents the presence of strain in the lattice. The lattice parameters of modified $BaTiO_3$ was calculated to be around $a = 3.91$ Å and $c = 3.99$ Å. The *c/a* ratio of $BaTiO_3$ and modified $BaTiO_3$ was found to be ~1.038 and ~1.02, respectively, which indicated the decrease in the tetragonality in modified $BaTiO_3$. Modified $BaTiO_3$ induces less displacement of Ti and O ions along c-axis and thereby increases the cubic phase [25]. XRD study was correlated further with Raman spectroscopy data. Raman scattering of $BaTiO_3$ and modified $BaTiO_3$ were performed and shown in figure 2. The phonon active modes of $BaTiO_3$ are observed at 184 (Al(LO)), 308 (B1, E(TO+LO)), 512 (Al(TO), E(TO)), 713 (Al(LO), E(LO)) and 250 cm^{-1}(Al(TO), E(LO)). Raman spectra showed peaks at 250, 184 and 512 cm^{-1} indicated TO mode of Al symmetry, which comprises tetragonal and orthorhombic phases [26]. The coexistence of tetragonal and orthorhombic phases is well-matched with XRD results. The sharp peak at 184 cm^{-1} indicated the presence of orthorhombic phase. Peak broadening and weakening in modified $BaTiO_3$ compared to $BaTiO_3$ showed lesser displacement of Ti and O atoms, which diminished tetragonal and orthorhombic phases due to the reduction of particle size [27]. Also, shifting of peaks in modified $BaTiO_3$ is attributed to the smaller particle size and induced stress [28].

3.2 *Microscopic studies*

Figure 3 shows scanning electron microscope (SEM) images of $BaTiO_3$ and modified $BaTiO_3$ nanoparticles. Morphology results confirmed the polyhedral microstructure with reduced particle size in modified $BaTiO_3$ than unmodified $BaTiO_3$. Formation of polyhedral morphology can be explained by following the dissolution–recrystallization mechanism, where aid of surfactant and initial dissolution of metal

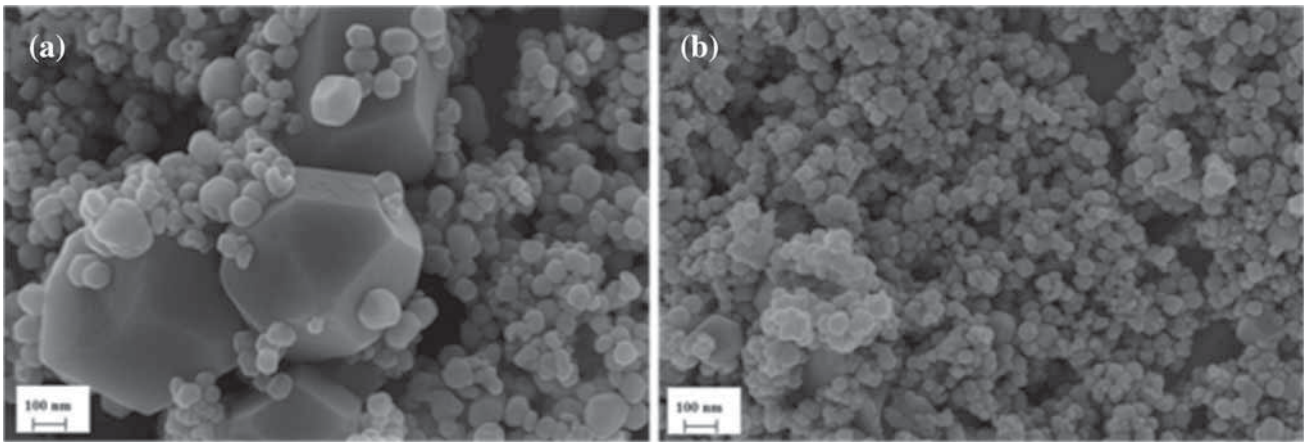

Figure 3. SEM images of (**a**) $BaTiO_3$ and (**b**) modified $BaTiO_3$.

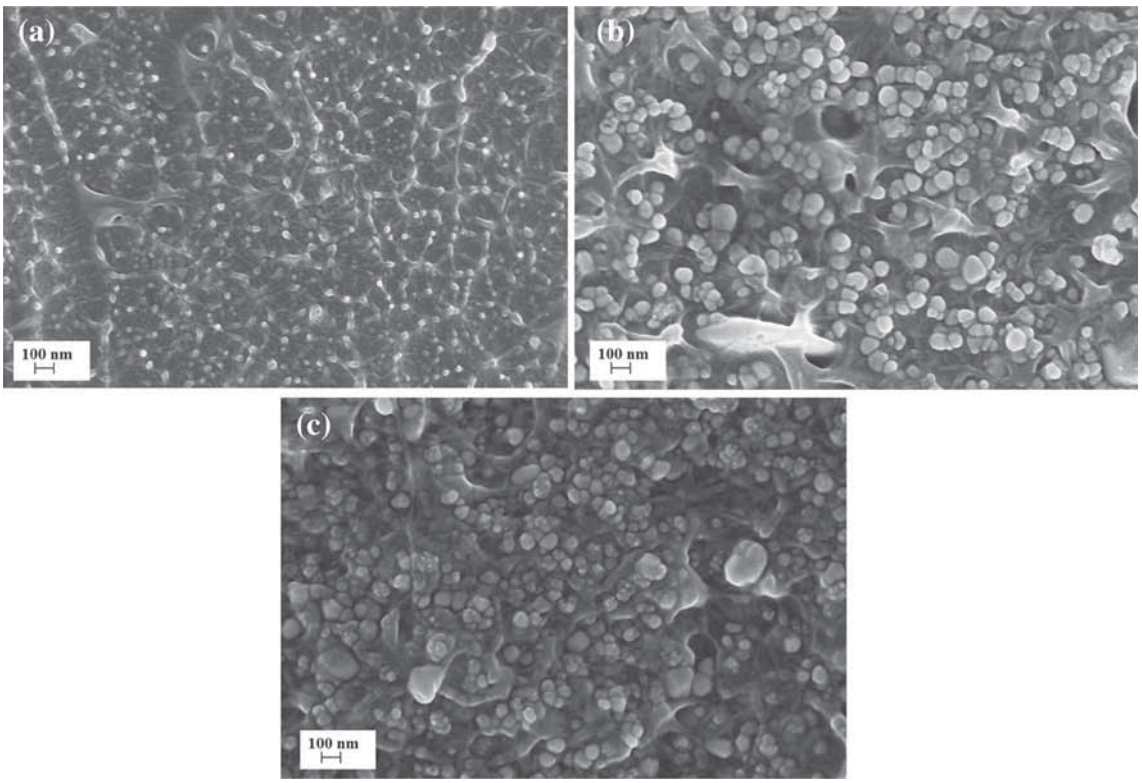

Figure 4. SEM images of (**a**) Pure PVDF–HFP, (**b**) PVDF–HFP/$BaTiO_3$ and (**c**) PVDF–HFP/modified $BaTiO_3$.

precursors form gel. The surfactant (PEG) plays a vital role during the recrystallization to stabilize $BaTiO_3$ in polyhedral morphology due to the interaction of functional groups of PEG with the high energy facet of the crystal to lower down its growth [18]. Faceting of crystal in the (110) plane gives rise to the polyhedral shape due to the adsorption of polyethylene glycol. Also, there is a significant size variation in unmodified $BaTiO_3$. However, size variation was reduced and average particle size calculated was 50 nm for the modified $BaTiO_3$. The modification of $BaTiO_3$ shows reduction in particle size due to the induced lattice disorder and increases the symmetric phase by hindering the growth [29]. The changes in the particle size is responsible for the reduction of tetragonal and orthorhombic phases in modified $BaTiO_3$ [30]. Figure 4 shows SEM micrographs of nanocomposites, which show homogeneous dispersion of fillers in polymer matrix. Further, microscopic studies suggest well-dispersion of modified $BaTiO_3$ in polymer matrix due to the reduction in particle size with high

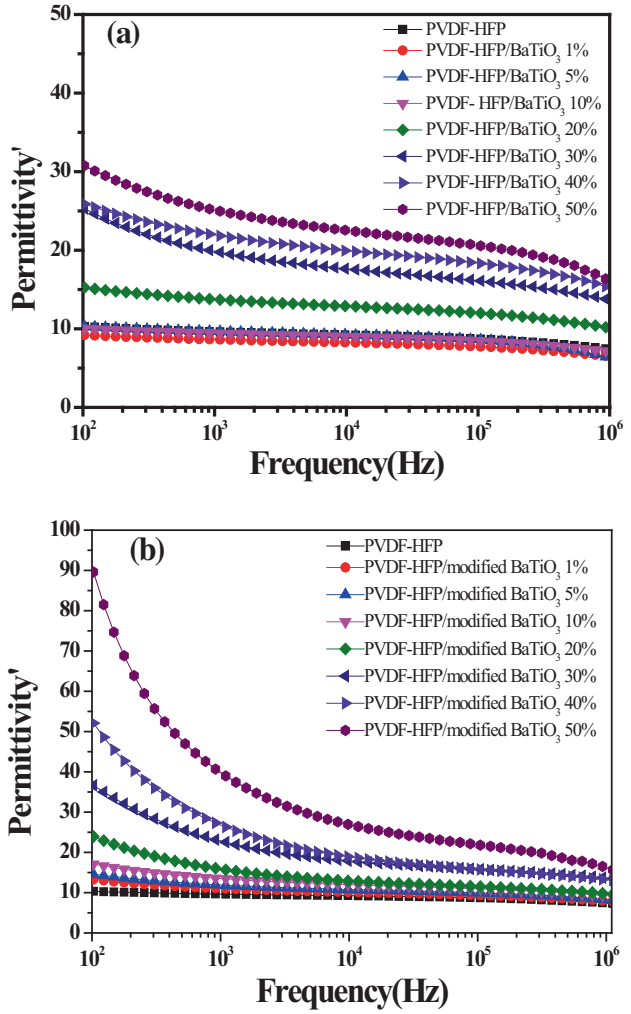

Figure 5. Frequency-dependent dielectric permittivity of (**a**) PVDF–HFP/$BaTiO_3$ and (**b**) PVDF–HFP/modified $BaTiO_3$.

active surface area as compared to unmodified $BaTiO_3$ nanoparticles.

3.3 *Dielectric studies*

Frequency-dependent dielectric studies of nanocomposite films were carried out and shown in figure 5. Figure 5a shows enhancement in the dielectric constant of PVDF–HFP with increase in the loading percentage of $BaTiO_3$. However, higher dielectric constant (~90 at 100 Hz) was achieved by loading modified $BaTiO_3$ filler in PVDF–HFP and shown in figure 5b. The enhancement in the dielectric constant is attributed to high interface polarization due to higher filler content in the PVDF–HFP matrix. Modification of $BaTiO_3$ increases charge carriers due to the addition of carbon and showed strong interaction and produce polarization, leading to higher dielectric constant. As per the earlier report, the particle size <100 nm posseses cubic crystal structure and >100 nm crystal structure transforms into tetragonal giving

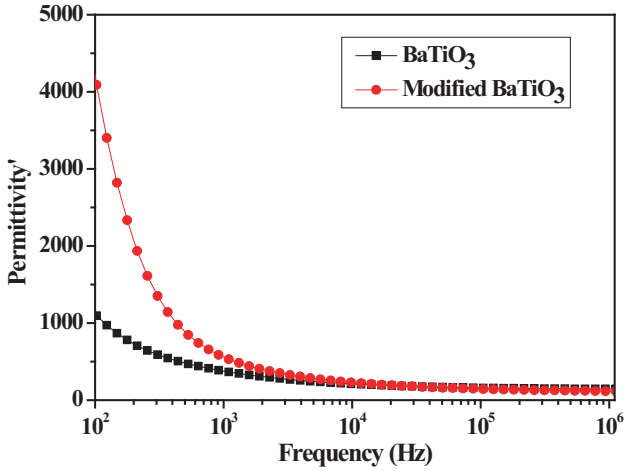

Figure 6. Frequency-dependent dielectric permittivity of $BaTiO_3$ and modified $BaTiO_3$.

rise to ferroelectric behaviour of $BaTiO_3$ nanoparticle [31], resulting in spontaneous polarization leading to high dielectric constant. However, reduction in particle size of modified $BaTiO_3$ (50 nm) exhibited higher interface polarization due to high surface area and showed higher dielectric constant at low frequencies than unmodified $BaTiO_3$. Dielectric properties of $BaTiO_3$ and modified $BaTiO_3$ were measured and shown in figure 6. The ceramic fillers were pressed into pellet (13 mm diameter) and coated with silver paste on both sides and placed between gold-plated electrodes to measure dielectric properties. As predicted, the permittivity of modified $BaTiO_3$ was higher than unmodified $BaTiO_3$ and exhibited strong interfacial polarization at lower frequencies (<1000 Hz). The observed dielectric behaviour of composite is evidenced further through Maxwell–Garnet model [32].

$$\varepsilon_{\text{eff}} = \frac{(2f+1)\varepsilon_{\text{f}} + 2(1-f)\varepsilon_{\text{m}}}{(1-f)\varepsilon_{\text{f}} + (2+f)\varepsilon_{\text{m}}}\varepsilon_{\text{m}}, \tag{1}$$

where ε_{eff}, ε_{f} and ε_{m} are the dielectric permittivities of composite, filler and matrix, respectively. Dielectric constants used around 1100 and 10 for barium titanate and PVDF–HFP, respectively. Figure 7 shows experimental values of dielectric permittivity for the composite, where composites with fillers up to 20 wt.% are followed the Maxwell–Garnet model. Also, the slope of the curve suggested more filler–matrix interactions in PVDF–HFP/modified $BaTiO_3$ nanocomposite. Thereafter, electric modulus was plotted against frequency to understand more about interface polarization at lower frequency. Electric modulus is the inverse of complex relative permittivity and expressed as [33]

$$M^* = \frac{1}{\varepsilon^*} = \frac{1}{\varepsilon' - j\varepsilon''} = \frac{\varepsilon'}{\varepsilon'^2 + \varepsilon''^2} + j\frac{\varepsilon''}{\varepsilon'^2 + \varepsilon''^2} = M' + jM'', \tag{2}$$

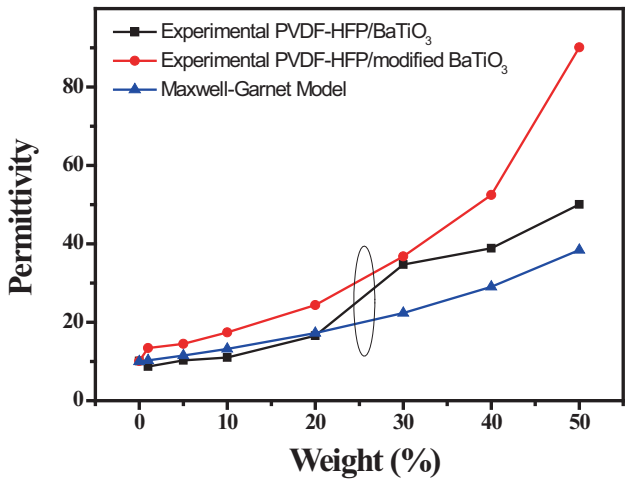

Figure 7. Comparison of dielectric permittivity of PVDF-based nanocomposite with theoretical model.

where the imaginary part (M'') of electric modulus interprets relaxation phenomena in composite films. Figure 8 evidences relaxation peak <100 Hz. The induced relaxation peak appeared for pure PVDF–HFP due to charge accumulation at the boundaries of amorphous and crystalline regions. Single relaxation peak was observed at lower frequency side and shifted towards higher frequency side with increasing filler percentage in the PVDF–HFP matrix and attributed to Maxwell–Wagner–Sillars (MWS) polarization, also known as interfacial polarization, which mostly exists in heterogeneous materials [34]. In comparison, PVDF–HFP/modified $BaTiO_3$ composite had shown predominant shifting of peak with increase in percentage of filler due to strong interfacial polarization. Also, addition of fillers in polymer matrix increased the dielectric loss due to dipolar loss, space charge migration and DC conduction. However, dielectric loss decreased with increase in frequency and become nearly constant at high frequency. The corresponding imaginary part of permittivity is shown in figure 9. Nonlinear behaviour was observed in the composite, which indicated the presence of conduction loss. At lower frequency, slight improvement in the linearity was observed in PVDF–HFP/modified $BaTiO_3$ nanocomposites than PVDF–HFP/$BaTiO_3$ nanocomposite, which clearly indicated more interface loss due to smaller particle size of modified $BaTiO_3$. Modification of $BaTiO_3$ showed well dispersion, strong interaction and stabilized $BaTiO_3$ in PVDF–HFP matrix, leading to strong interfacial polarization and reduced the dielectric mismatch between fillers and matrix. Again, temperature-dependent dielectric studies were carried out from −40 to 130°C and shown in figure 10. Two different relaxation peaks were identified in M'' curves in both the lower and higher temperature sides. The low temperature broad relaxation peak is attributed to crystalline behaviour of the polymer. The relaxation peak at higher temperature side is attributed to MWS polarization. The intensity of the relaxation peak increased and peak broadening

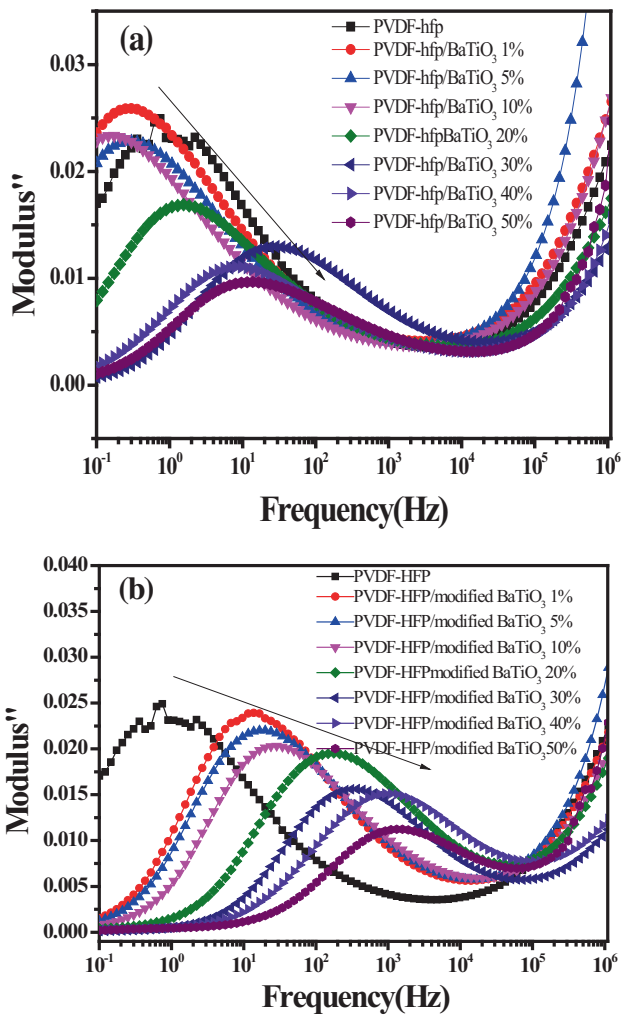

Figure 8. Imaginary part of dielectric modulus against frequency of (**a**) PVDF–HFP/$BaTiO_3$ and (**b**) PVDF–HFP/modified $BaTiO_3$.

decreased with temperature, which ascribed to asymmetric nature of MWS relaxation. Shift in the modulus (M'') peak with increase in temperature of the composite indicated faster dipole vibration and orientation against changing electric field. Similar type of dielectric relaxations were observed earlier in PVDF-based nanocomposites [34,35]. Temperature dependence of dipolar polarization is also confirmed by calculating the activation energy, and the graph shown in figure 11 suggested Arrhenius behaviour. Activation energy was calculated by using the following formula:

$$f = f_0 \exp\left(-\frac{E_a}{kT}\right), \tag{3}$$

where E_a represents activation energy, k the Boltzman constant and T the absolute temperature. Activation energies are determined to be 0.9, 0.59 and 0.52 meV for PVDF–HFP, PVDF–HFP/$BaTiO_3$ and PVDF–HFP/modified $BaTiO_3$, respectively. This decrease in activation energy value

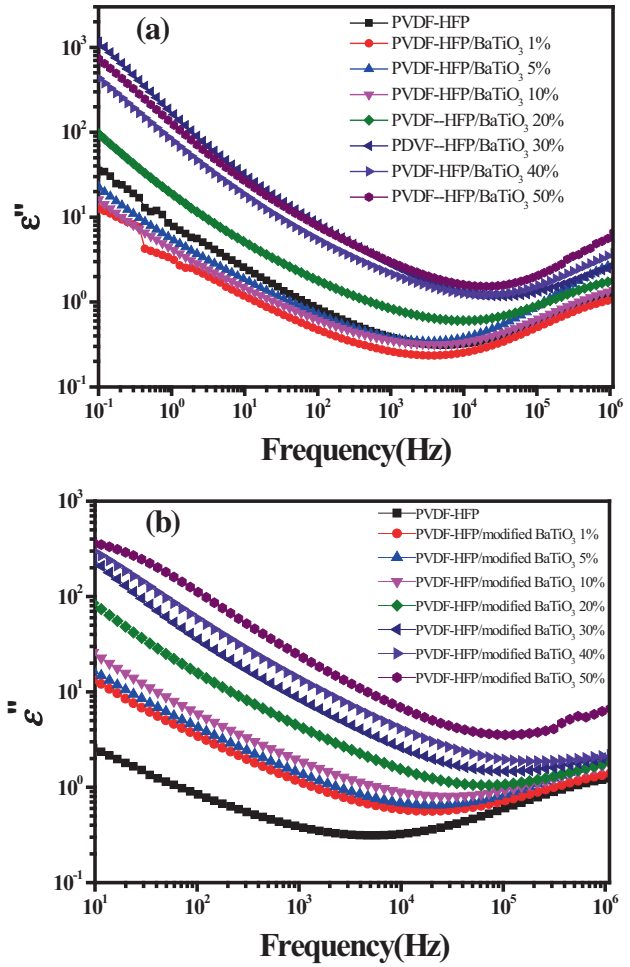

Figure 9. Imaginary part of dielectric permittivity against frequencies of (**a**) PVDF–HFP/$BaTiO_3$ and (**b**) PVDF–HFP/modified $BaTiO_3$.

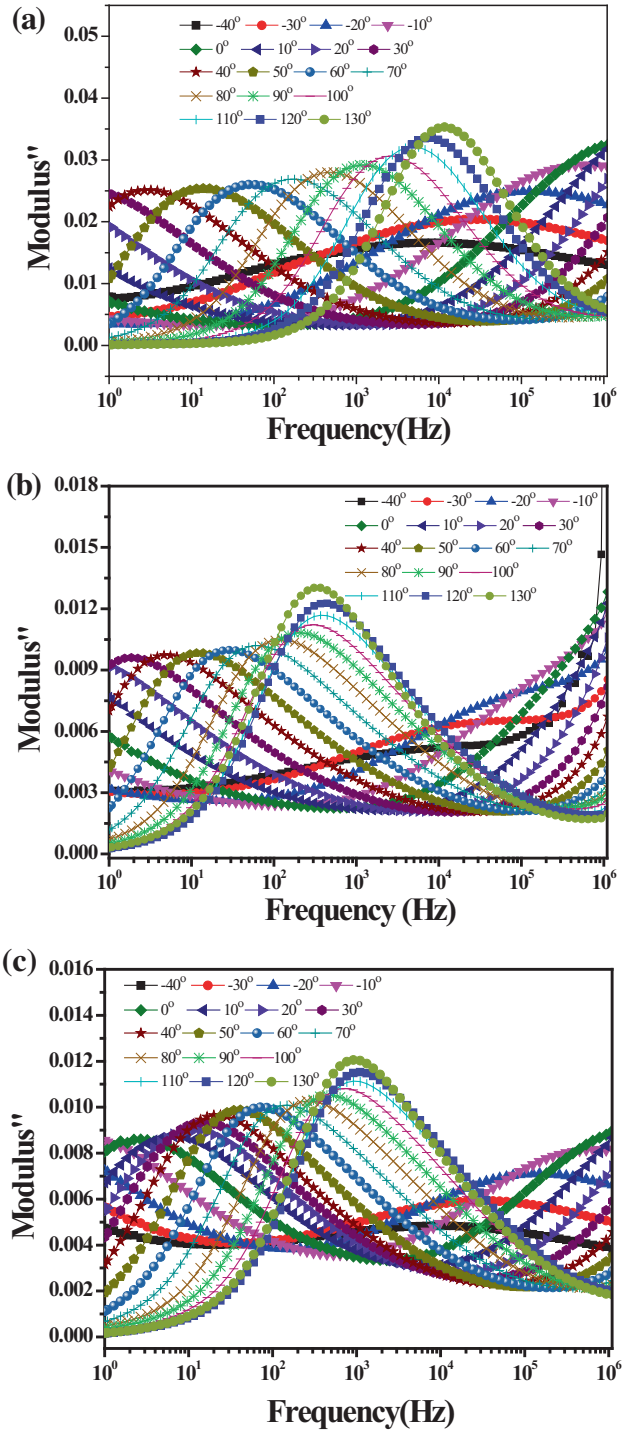

Figure 10. Frequency-dependent imaginary part of electric moduli of (**a**) PVDF–HFP, (**b**) PVDF–HFP/$BaTiO_3$ and (**c**) PVDF–HFP/modified $BaTiO_3$ at various temperatures.

suggested the improvement in mobility of charge carriers at interfaces in the composite compared to pure PVDF–HFP.

Thereafter, the developed nanocomposite films were used to fabricate an electromechanical sensing device. The nanocomposite films with 20 × 20 mm in size were sputter-coated on both sides with gold. The films were sandwiched with Cu tape with electrical contacts. To make the device robust, the device was sealed by polyamide tape. The device was propelled under corona with the applied voltage of 15 kV and temperature of 60°C for 1 h to observe the electromechanical response. In general, the capacitance changes by changing the electrode spacing. Thus, the device undergoes geometrical change due to the reduction of electrode spacing under various static loads. Hence, sputter-coated film was placed between metallic electrodes like a parallel plate capacitor to measure the change in capacitance under various loads (static). Figure 12 shows the change in capacitance ($\Delta C/C_o$) against applied load in the developed device. Herein, C_o is the capacitance at no load condition and ΔC is the capacitance difference under loading. The average capacitance was measured and reported at 1 kHz. The significant change in the capacitance was observed in modified $BaTiO_3$-based nanocomposite device than unmodified $BaTiO_3$-based composite and pure polymer device. Both the nanocomposite devices exhibited higher sensitivity than that of the device

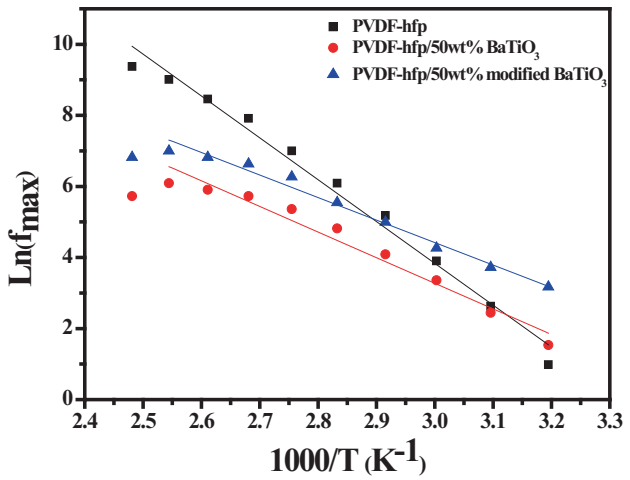

Figure 11. Activation energy plots of PVDF–HFP-based nanocomposite.

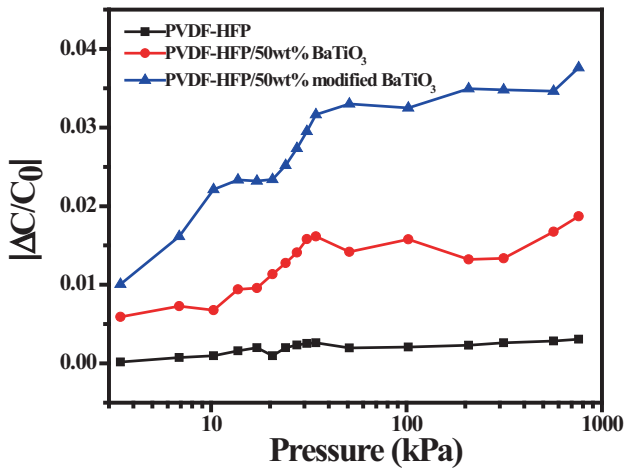

Figure 12. Change in capacitance response of the device against various loads.

made by PVDF–HFP film. The difference in capacitance of the composite is attributed not only to the electrode spacing, but also to the polarization caused by the addition of fillers in the polymer matrix, which stimulated the relative ionic movement. Similar type of result was observed in previously reported polymer-based nanocomposite [12,36]. Overall, the modified PVDF–HFP/$BaTiO_3$ nanocomposite with enhanced dielectric properties might be useful to build the electromechanical sensing device.

4. Conclusion

Fluoro-polymer based nanocomposites were prepared by solution-casting method by incorporating $BaTiO_3$ and modified $BaTiO_3$. Modification of $BaTiO_3$ was carried out successfully by using electrochemically prepared carbon solution. Structural characterization reveals the coexistence of orthorhombic and tetragonal phases in both $BaTiO_3$ and modified $BaTiO_3$. Polygonal shape was confirmed through microscopy and also significant reduction of particle size was observed in modified $BaTiO_3$ than unmodified $BaTiO_3$. Dielectric behaviour was investigated for the nanocomposite and showed significant increase in dielectric constant in PVDF–HFP/modified $BaTiO_3$ than PVDF–HFP/$BaTiO_3$. Also, PVDF–HFP/modified $BaTiO_3$ showed more interfacial polarization and reduced dielectric loss than PVDF–HFP/$BaTiO_3$ and PVDF–HFP. Furthermore, the developed films were used as dielectric layer to fabricate a capacitive pressure sensor device. Overall, PVDF–HFP/modified $BaTiO_3$ composite device exhibited higher sensing response to the applied load.

References

[1] Nayak S, Kumar T and Khastgir D 2016 *Ceram. Int.* **42** 14490
[2] Arlt G, Hennings D and With G D 1985 *J. Appl. Phys.* **58** 1619
[3] Nayak S, Sahoo B, Chaki K and Khastgir D 2014 *RSC Adv.* **4** 1212
[4] Haertling G H 1999 *J. Am. Ceram. Soc.* **82** 797
[5] Landeros J O, Yanez C G, Juarez R L, Velasco I D and Pfeiffer H 2012 *J. Adv. Ceram.* **1** 204
[6] Moon J, Suvaci E, Morrone A, Costantino S A and Adair J H 2003 *J. Eur. Ceram. Soc.* **23** 2153
[7] Lin M F, Thakur V K, Tan E J and Lee P S 2011 *RSC Adv.* **1** 576
[8] Yang K, Huang X, Liu F and Jiang P 2013 *IEEE international conference on solid dielectrics (ICSD)* p 722
[9] Dalle Vacche S D, Oliveira F, Leterrier Y, Michaud V, Damjanovic D and Manson J A E 2014 *J. Mater. Sci.* **49** 4552
[10] Jung H M, Kang J H, Yang S Y, Won J C and Kim Y S 2010 *Chem. Mater.* **22** 450
[11] Tang H, Zhou Z and Sodano H A 2014 *ACS App. Mater. Int.* **6** 5450
[12] Nayak S, Chaki T K and Khastgir D 2014 *Ind. Eng. Chem. Res.* **53** 14982
[13] Yang J, Zhang J, Liang C, Wang M, Zhao P, Liu M *et al* 2013 *ACS App. Mater. Int.* **5** 7146
[14] Beier C W, Cuevas M A and Brutchey R L 2010 *Langmuir* **26** 5067
[15] Xie L, Huang X, Huang Y, Yang K and Jiang P 2013 *ACS App. Mater. Int.* **5** 1747
[16] Kim P, Jones S C, Hotchkiss P J, Haddock J N, Kippelen B, Marder S R *et al* 2007 *Adv. Mater.* **19** 1001
[17] Yang K, Huang X, Huang Y, Xie L and Jiang P 2013 *Chem. Mater.* **25** 2327
[18] Dong L, Shi H, Cheng K, Wang Q, Weng W and Han W 2014 *Nano Res.* **7** 1311
[19] Fu J, Hou Y, Zheng M, Wei Q, Zhu M and Yan H 2015 *ACS Appl. Mater. Interf.* **7** 24480
[20] Wu C, Huang X, Wu X, Yu J, Xie L and Jiang P 2012 *Comp. Sci. Tech.* **72** 521
[21] Chen Q, Jin L, Weng W, Han G and Du P 2008 *Sur. Rev. Lett.* **15** 19
[22] Niu Y, Yu K, Bai Y and Wang H 2015 *IEEE Trans. Ultrason. Ferroelec. Freq. Control* **62** 108

[23] Li H, He X, Kang Z, Huang H, Liu Y, Liu J *et al* 2010 *Angew. Chem. Int. Ed.* **49** 4430
[24] Hammer M and Hoffmann M J 1998 *J. Elect. Ceram*. **2** 75
[25] Rabuffetti F A and Brutchey R L 2012 *J. Am. Chem. Soc.* **134** 9475
[26] Qi J Q, Peng T, Hu Y M, Sun L,Wang Y, Chen W P *et al* 2011 *Nano Sci. Res. Lett.* **6** 466
[27] Huang T C, Wang M T and Sheu H S 2007 *J. Phys. Condens. Mater.* **19** 1
[28] Dobal P S, Dixit A, Katiyar R S, Yu Z, Guo R and Bhalla A S 2001 *J. Appl. Phys.* **89** 8085
[29] Aepuru R, Kankash S and Panda H S 2016 *RSC Adv.* **6** 32272
[30] Mao Y P, Mao S Y, Ye Z G, Xie Z X and Zheng L S 2010 *J. Appl. Phys.* **108** 014102
[31] Dang Z M, Xu H P and Wang H Y 2007 *Appl. Phys. Lett.* **90** 012901
[32] Fan B H, Zha J W, Wang D R, Zhao J and Dang Z M 2012 *Appl. Phys. Lett*. **100** 092903
[33] Tian F and Ohki Y 2014 *IEEE Trans. Dielec. Elec. Insulat.* **21** 929
[34] Chanmal C V and Jog J P 2008 *Exp. Polym. Lett.* **2** 294
[35] Aepuru R, Rao B V B, Kale S N and Panda H S 2015 *Mater. Chem. Phys*. **167** 61
[36] Aepuru R and Panda H S 2016 *J. Phys. Chem. C* **120** 4813